# A Methodology for Predicting Improved Dipole Source Configurations From Near-Field Scan Data

Hossein Rezaei<sup>®</sup>, *Member, IEEE*, Xin Yan<sup>®</sup>, *Graduate Student Member, IEEE*, David J. Pommerenke<sup>®</sup>, *Fellow, IEEE*, and Daryl G. Beetner<sup>®</sup>, *Senior Member, IEEE* 

Abstract—Equivalent sources found from near-electric and magnetic field scans are often used to predict and solve interference problems. While there are many ways to represent the source, the user lacks the ability to determine which of the many possible source configurations is more likely to represent the "true" source, and thus accurately represent field data outside the measurement area and in the presence of typical measurement errors. A methodology is proposed for estimating which of many possible dipole source representations of near-field scan data are likely to give better estimates of fields outside the measurement scan plane when utilizing imperfect measurement data. A quality metric for determining better configurations is proposed, which utilizes the statistical variation of the global difference measure (GDM) in the predicted and measured fields. Equivalent sources are estimated when adding noise to measurement data, and prediction statistics are generated for multiple instantiations of measured noise. Results demonstrate that the better configurations minimize the average plus standard deviation of the GDM. The ability of the technique to identify robust source configurations was tested when measurements were subject to additive measurement noise, cross-field coupling, and systematic errors in probe position, and was evaluated based on its ability to predict fields at points above and to the side of the measurement plane. The method consistently identified better source configurations using both simulated and measured data.

Index Terms—Dipole, least squares method, near-field scan, RF interference, source representation.

#### I. INTRODUCTION

REDICTION of the near electric and magnetic fields generated by electrical components can be used to mitigate potential radiofrequency interference (RFI) problems early in the design process. Near-field scanning is commonly used to

Manuscript received 22 January 2023; revised 15 March 2023 and 22 April 2023; accepted 4 May 2023. This work was supported by the National Science Foundation (NSF) under Grant IIP-1916535. (Corresponding author: Hossein Rezaei.)

Hossein Rezaei and Xin Yan are with the Electrical Engineering Department, Missouri University of Science and Technology, Rolla, MO 65401 USA (e-mail: hossein.rezaei@ieee.org; yx9n9@mst.edu).

David J. Pommerenke is with the Graz University of Technology, 8010 Graz, Austria, and also with Silicon Austria Lab's Graz EMC Lab, 8010 Graz, Austria (e-mail: david.pommerenke@tugraz.at).

Daryl G. Beetner is with the Electrical and Computer Engineering Department, Missouri University of Science and Technology, Rolla, MO 65409 USA (e-mail: daryl@mst.edu).

Color versions of one or more figures in this article are available at https://doi.org/10.1109/TEMC.2023.3274491.

Digital Object Identifier 10.1109/TEMC.2023.3274491

characterize RFI noise sources. An equivalent source representation can be found using equivalent dipoles with a least squares method (LSQ) [1], [2], [3]. An equivalent dipole model represents the source with several dipoles placed throughout the source domain [1], [2], [3]. The magnitude and phase of dipoles at fixed locations can be found using the least squares method with regularization from the near-field scanning data [1], [4]. Genetic algorithms (GAs) and differential evolution (DE) can be used to find the location of dipoles if the user does not know the source location [5], [6], [7], [8], [9].

A survey of the literature related to source reconstruction studies was performed and analyzed with respect to the reconstruction methodology, the frequency range, the types of noise that were investigated, and the type, location, and number/density of the inferred sources. The results are summarized in Table I [2], [3], [5], [6], [7], [8], [9], [10], [11], [12], [13], [14], [15], [16], [17], [18], [19], [20], [21], [22], [23], [24], [25], [26]. Approaches typically used a dipole or current distribution based source. Most methods were validated for just one frequency or over a relatively narrow range of frequencies. In many cases, the robustness of the approach was not tested against measurement errors. When errors were included, it was most common to add Gaussian white noise to measured or simulated data to represent instrumentation noise. Position error causes a systematic error throughout the measurement. The sensitivity of amplitude only or phase resolved near field measurements to position error was addressed in [27] and [28]. Although several methods exist to solve the source reconstruction problem for RFI applications, and many source configurations have been studied, the user does not have an effective method of judging which source representations will most accurately represent fields outside the scan area for RFI applications [13], [18]. The least square error between the measured fields used to estimate the source and the reconstructed fields is not necessarily sufficient when the measurements are corrupted with noise and other measurement errors [29].

No exact theoretical criteria exist for choosing the source for an inverse problem when predefined information about the source is unavailable. Most papers leave the source definition to the user. As a result, the user is left with the dilemma of determining which source configuration, out of the many possible solutions, will do a good job of predicting fields at locations outside the scan plan for the RFI application [13], [18].

In this article, a method is proposed for finding which dipole representation among several candidate configurations is likely

0018-9375 © 2023 IEEE. Personal use is permitted, but republication/redistribution requires IEEE permission. See https://www.ieee.org/publications/rights/index.html for more information.

TABLE I SUMMARY OF EXISTING FIELD RECONSTRUCTION STUDIES

Ref.	Method (DUT)	F (GHz)	Method	Measurement errors considered?	Source definition
This	Equivalent	0.001-	LSQ with	Cross-coupling,	Used quality metrics to
work	Dipole (IC, transformer)	18	quality metric	position error, random noise	find a good source combination
[2]	Dipole moment	0.87 and	Iterative	None	24 dipoles in the x- and
[2]	(buffer IC)	5	riciative	TVOIC	y-directions with a gap
					of 5 mm
[3]	Microcontroller	0.028	Electric	None	Defined by user
		and 0.04	and magnetic		
		0.01	dipoles		
[5]	Dipole method	≈ 1.6	LSQ and	None	GA found number of
	(Clock buffer IC)		GA		dipoles and their location.
[6]-	Dipole method	0.5,1,	Dipoles	None	DE found the location and
[9]	(trace and IC)	8.8	with DE		the number of dipoles.
[10]	Clock	0.867	Iterative	White Gaussian	11 dipoles in the x- and
	chip circuit			noises	y-directions with a gap of 4 mm
[11]	Equivalent	1,<0.1	Iterative	Different SNR	The equivalent magnetic
. ,	current (Trace	,			current is set equal to
	and dc-dc				the area of the scanning plane and is divided
	buck converter)				into 48 × 38 elements
					by a square grid with a
					side length of 0.75 mm
[12]	Dipole moment (IGBT and a	< 0.1	Iterative	None	GA found dipole
	power diode)				moment, position, and orientation.
[13]	Huygens' box	<6	LSQ	None	9 dipoles in the x-direction
	and dipole				and 8 dipoles in the y
	(patch antenna and IC)				directions with a gap of 4 mm and 21 dipoles in the
	una re)				x and y directions with a
					gap of 3 mm
[14]	Current	< 0.1	Iterative	None	Defined by user
	distribution (dc-dc				
	converter)				
[15]	Current	1	LSQ	5% of white	Discretized source
	distribution (The CK505			noise	plane to 61 × 61 pixels
	die)				
[16]	Current	20	Iterative	Different SNR	Discretized source
	distribution				plane (55 × 55) with a
	(Transmission Lines)				gap of 1 mm
[17]	Dipole moment	0.45	LSQ	None	Quantified guidelines
	(a trace and				to find the height, source
	PLL IC)				spacing, and scanning spacing.
[18]	Huygens' box	2-3	LSQ	None	8 dipoles in the x and
	and equivalent				y directions with a gap
	dipoles				of 4 mm
	(Patch antenna & trace)				
[19]	Current source	5.8	MoM	White noise	Discretized source
	(trace & CBS	and 20		SNR=30 dB	plane (55 × 55) with a
[20]	antenna)  Dipole method	2.5	LSQ	None	gap of 1 mm 8 dipoles in the x-direction
[20]	(two patch	2.3	LOV	TAOHE	(gap of 5 mm) and 8
	antennas)				dipoles in the y-directions
F213	Pil	2.2	The section	Nimi	(gap of 6 mm)
[21]	Equivalent dipole (a patch	2.2	Iterative with	None	Dipole moment, and the locations, and numbers
	antenna with		artificial		of all dipoles were
	four metallic		neural		found
[22]-	surroundings) Equivalent	2.2	networks Artificial	None	Dipole moment, the
[22]-	Equivalent Dipole	2.2	neural	NOHE	locations, and numbers of
[]	-r		network		all dipoles were found
			with		
[26]	Equivalent	2-3	iteration Machine	Random noise	Dipole moment,
[20]	Dipole		learning	in a simulation	location, and number
	_		-	example	are obtained with
L					machine learning

to yield the most accurate representation of fields outside of the measurement area and is likely to be robust to typical measurement errors like measurement noise in the scan data, errors in scan height, and cross-coupling between electric and magnetic field measurements. A quality metric is proposed which helps to identify these configurations based on the statistical variation

of the global difference measure (GDM) in the predicted and measured fields found when adding typical errors to the measured data [30]. The process for reconstructing dipole sources is reviewed in Section II. The quality metric and process for finding better source configurations is introduced in Section III. The ability of the approach to find source configurations that predict fields well at locations outside of the scan area (above and to the side of the measurement plane for RFI applications [13], [18]) was tested through the simulation of two test cases in Section IV and through measurement in Section V. The test cases have either electric or magnetic field dominant sources, or a combination of the two over a broad frequency range and include both electrically small and large structures. Results show that the proposed quality metric was consistently minimized for those configurations that also best predicted fields outside the measurement plane. Finally, Section VII concludes this article.

### II. DIPOLE-BASED SOURCE RECONSTRUCTION METHOD

A dipole representation of near-field sources can be found starting with the vector potential formulation [1], [2], [3]:

$$\bar{A}(\bar{r}) = \frac{\mu_0}{4\pi} \int_v \bar{J}(\bar{r}') \frac{e^{-jk_0|\bar{r}-\bar{r}'|}}{|\bar{r}-\bar{r}'|} dv'$$
 (1)

where A is the magnetic vector potential, J is the source current,  $k=\omega\sqrt{\varepsilon\mu}=2\pi/\lambda$  is the wavenumber, and  $\lambda$  is the wavelength. The permeability and permittivity of the surrounding medium are  $\mu$  and  $\varepsilon$ , respectively, and  $\vec{r}-\vec{r'}$  is a vector between an arbitrary observation point r and a source point r' in domain v. Both r and r' are defined with respect to the origin 0. The electric and magnetic fields can be calculated from the magnetic vector potential as [2]

$$\mu_0 \bar{H} \ (\bar{r}) = \nabla \times \bar{A} (\bar{r}) \tag{2}$$

$$i\omega\varepsilon_0\bar{E}\ (\bar{r}) = \nabla\times\bar{H}(\bar{r}).$$
 (3)

The sources are considered to be infinitesimally small electric and magnetic dipoles. The electric dipole moment is defined as  $\bar{P}$ , and the magnetic dipole moment as  $\bar{M}$  [1], [2], [3]. The electromagnetic fields which radiate from electric and magnetic dipoles are given by [1], [2], [3]

$$[E_x ; E_y ; H_x ; H_y] = [T] \times [P_x ; P_y ; P_z ; M_x ; M_y ; M_z]$$
(4)

where  $E_x$  or  $H_x$  and  $E_y$  or  $H_y$  are the x and y components of the electric and magnetic fields, respectively. The contribution of each dipole to corresponding field components is represented using the T matrix (e.g.,  $T_{Hx,Px}$  represents the  $H_x$  field component which is generated with the  $P_x$  dipole). The unknown electric and magnetic dipoles can be found from known field measurements using LSQ as [1], [2], [3]

$$[P_x \ P_y \ P_z \ M_x \ M_y \ M_z] = [T'T]^{-1} \times T' \times [E_x \ E_y \ H_x \ H_y]$$

where T is the field generation matrix given in (4) [1], [2], [3], and T' is its conjugate transpose.

A typical source representation would place the electric and magnetic dipoles on an xy plane just above the device whose

emissions they are intended to represent. This plane will be called the source plane. The transfer function matrix [T] can be calculated between the source plane and an observation point outside a volume containing the dipoles and the device, for example, on a plane above or to the side of the device under test (DUT).

The inferred sources create a field in the scan plane which does not exactly match the measured fields in this plane. The quality of the match needs to be defined. This error definition can then be applied to fields in planes other than the measurement plane.

There are two common approaches to quantifying the error in the predicted fields: using the root-mean-square error in the predicted fields at known measurement points [1] and using feature selective validation (FSV) [30]. FSV was created by an IEEE standard committee as a reference method and is widely used in the electromagnetic compatibility community [30].

FSV determines a figure of merit that is roughly equivalent to a visual comparison of the measured and predicted data by a human observer. The output of FSV is found from a point-by-point comparison and is represented in the form of the amplitude difference measure (ADM) or feature difference measure (FDM), which represents the feature differences between data sets. The combination of ADM and FDM is reflected in GDM. The comparison is considered to be Excellent for GDM  $\leq$  0.1, Very Good for 0.1  $\leq$  GDM < 0.2, Good for 0.2  $\leq$  GDM < 0.4, Fair for 0.4  $\leq$  GDM < 0.8, Poor for 0.8  $\leq$  GDM < 1.6, and Very Poor for 1.6  $\leq$  GDM [30], which makes the comparison much easier for the user.

## III. DETERMINING BETTER SOURCE CONFIGURATIONS

Uncompensated errors in the measurement will reduce the accuracy of the predicted fields. There are three main sources of error in near-field scanning: cross-field coupling, position error, and random noise in the measured field levels. The impact of each noise type will be considered using simulations in the following study.

Cross-field coupling is caused when the near-field measurement probes are sensitive to more than one field component. In a real measurement, H-field probes also detect the E-field, and E-field probes detect the H-field, causing errors in the measured field components [31]. The cross-coupling becomes worse at higher frequencies, especially above 1 GHz. To consider cross-coupling effects up to 30% of the unwanted field ( $\approx$ –10.5 dB suppression) has been added to the simulated field measurements in the following experiments.

Position error is caused by a systematic error in the probe position throughout the scan [27], [28]. In the simulation, the position of each E-field or H-field point has been shifted by 1.5 mm. The position error can distort the phase distribution [29] as well as the magnitude of the measured fields. Up to a 1.5 mm position error has been considered when creating "measured" field data in simulations.

Additive random noise in the measured field levels is caused primarily by quantization errors in the measurement instrument or by thermal noise within the system. This error is represented here by setting the effective noise floor of the measurement such that the maximum signal-to-noise ratio (SNR) at any point throughout the scan is SNR  $\approx 15$  dB. The phase is random, but the signal is noise floor limited when referenced against the maximum field strength.

All three errors were set to cause rather severe distortion of the actual field data. Actual systems will typically achieve better SNR, especially if the user can set the source strength. A 1.5 mm position error is rather large. Position error includes not only the mechanical position error but the difference between the physical center of the probe and its electrical center. Probe factor errors have not been considered as they remain constant throughout all scanning and would just cause a fixed offset in the magnitude of the measured field.

These noise sources will be used later in this work to demonstrate a methodology for finding a near-optimal dipole representation of an RFI source. The reconstruction method will be repeated with different values of the three types of noise sources to investigate the robustness of the reconstruction method.

To find a near-optimal dipole representation, we propose to find a dipole combination with relatively low values of GDM, and the standard deviation of the GDM over multiple applications of the approach while adding different values of random noise to the scan data. The standard deviation of GDM over its population determines how stable the GDM value is against variations of the captured field plane data and can be calculated as

$$STD (GDM) = \sqrt{\frac{\sum (GDM_i - \mu)^2}{N}}$$
 (6)

where  $\mu$  is the mean value of GDM and N is the size of GDM samples. Experimental evidence suggests that a solution, defined as several sources at given locations, which leads to stable GDM even if the capture plane data are varied is often a better solution compared to a solution that will show highly varying GDM if capture plane data are slightly different. While solutions could be significantly improved with access to data beyond the scanned fields, like the value of fields to the side of the DUT, and the value of fields on other planes, it is assumed the user only knows the scan data in the plane above the DUT. Using these measures, we propose the following process for determining the near-optimal configuration of the equivalent dipoles.

1) Given the noisy scanning data above the DUT corrupted with additive random noise, cross-field coupling noise, and position error, for example:

$$E_{p}(x, y, z) = E(x + \Delta x, y + \Delta y, z + \Delta z) + n(x, y, z) + \frac{\alpha_{i}}{\zeta} H(x, y, z)$$
(7)

where  $\Delta x, \Delta y$ , and  $\Delta z$  are position errors,  $\zeta$  is the characteristic impedance of free space, and  $\alpha_i$  is the cross-coupling coefficient. Position error has been considered as a systematic error which means the position of each E-field or H-field point has been shifted by 1.5 mm. n(x, y, z) is additive random noise, simulating instrumentation noise, and as such is normally distributed. The noise amplitude was set to achieve a maximum SNR of 15 dB across the scan plane, whereas the noise power

remained constant from location to location. The noise phase was random.

- 2) Consider N different dipole configurations as source representations. Each dipole configuration has a different number of dipoles in the x and y directions as well as different spacing between them. Each source location includes six dipole components:  $P_x(x,y,z)$ ,  $P_y(x,y,z)$ ,  $P_z(x,y,z)$ ,  $M_x(x,y,z)$ ,  $M_y(x,y,z)$ , and  $M_z(x,y,z)$ .
- 3) Use least squares to determine the values of the dipoles for each configuration using (5).
- 4) Repeat steps 2 and 3 for M instantiations of random additive random noise to form an  $N \times M$  matrix of solutions (dipole combination versus additive noise) at each frequency.
- 5) Find those solutions which minimize the average and standard deviation of the GDM on the measurement plane overall "noisy" solutions, as defined by the quality metric  $\sigma$  as follows:

$$\begin{split} \sigma_i &= \text{GDM}_{\text{norm}} + \text{STD}(\text{GDM}_{\text{norm}}) \\ &= \frac{1}{4} \left[ \text{GDM}_{\text{Exi,norm}} + \text{GDM}_{\text{Eyi,norm}} \\ &+ \text{GDM}_{\text{Hxi,norm}} + \text{GDM}_{\text{Hyi,norm}} \right] \\ &+ \frac{1}{4} \left[ \text{STD}(\text{GDM}_{\text{Exi}})_{\text{norm}} + \text{STD}(\text{GDM}_{\text{Eyi}})_{\text{norm}} \\ &+ \text{STD}(\text{GDM}_{\text{Hxi}})_{\text{norm}} + \text{STD}(\text{GDM}_{\text{Hyi}})_{\text{norm}} \right] \end{aligned}$$

$$GDM_{Exi,norm} = \frac{\sum_{j=1}^{M} GDM_{Exi,j}}{\left(\sum_{j=1}^{M} GDM_{Exi,j}\right)_{max}}$$
(9)

 $\mathrm{STD}(\mathrm{GDM}_{\mathrm{Exi}})_{\mathrm{norm}}$ 

$$= \frac{\sqrt{\frac{\sum_{j=1}^{M} (\text{GDM}_{\text{Exi},j} - \text{GDM}_{\text{Exi},\text{avg}})^{2}}{M}}}{\sqrt{\sqrt{\frac{\sum_{j=1}^{M} (\text{GDM}_{\text{Exi},j} - \text{GDM}_{\text{Exi},\text{avg}})^{2}}{M}}}}_{\text{max}}.$$
 (10)

Those configurations which minimize the proposed quality metric  $\sigma$  will be shown in the following text to be more likely to accurately predict fields above and to the side of the measurement plane.

## IV. VERIFICATION THROUGH SIMULATION

The approach was verified using two different DUTs, an electromagnetic interference (EMI) filter and an IC with nearby traces. These configurations were built such that they would include both magnetic-field-dominated and electric-field-dominated sources and would allow testing over a wide frequency range. The accuracy of results is considered not only in the measurement plane but to the side and above the measurement plane.

## A. EMI Filter

Some unintentional radiators primarily create near magnetic fields, and some primarily create electric fields. An EMI filter is a

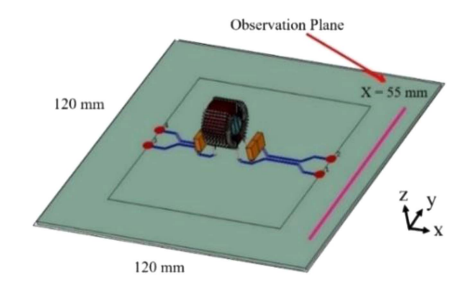


Fig. 1. EMI filter with ground plane (120 mm  $\times$  120 mm).

common source of the interference with a strong near magnetic field due to a physically large inductor creating interference, particularly at lower frequencies. The EMI filter shown in Fig. 1 was used to study such a source, focusing on emissions at 100 MHz. The large inductor and two capacitors occupy an area of  $20~\text{mm}\times25~\text{mm}$ . The large inductor generates a strong magnetic field, which may interfere with a nearby victim. The dimensions of the inductor were  $10~\text{mm}\times20~\text{mm}$  (0.003  $\lambda\times0.006$   $\lambda$  at 100~MHz). The dimensions of the ground plane were  $120~\text{mm}\times120~\text{mm}$  (0.04  $\lambda\times0.04~\lambda$  at 100~MHz). The input ports were excited with 100~MHz sinusoidal signals with magnitudes of 1 and -1.1~V (to have a  $180^\circ$  phase change). These inputs create both a differential and common mode excitation, to create a more realistic source.

An electromagnetic model for the EMI filter was developed as part of the work described in [32]. Electric and magnetic fields were simulated from this source in CST Studio Suites [33] and used to validate methods for predicting interference using the source reconstruction technique. Initially, the data were captured in a 120 mm × 120 mm observation plane at z = 50 mm above the ground plane, with step size 2 mm (i.e., there were 3721 measurements of  $E_x$ ,  $E_y$ ,  $H_x$ , and  $H_y$  within the plane). Cross-field coupling (about 30%) and random noise were added to the noiseless field so that the best SNR  $\approx$  15 dB. As shown in Fig. 2, the additive noise (cross-coupling and random noise) has more influence on the E field than the H field as the DUT is magnetic field dominant. This noisy data (see Fig. 2) were used to estimate the sources using (5). Two observation planes were used to validate the results. The secondary plane is mounted in the xy plane above the scan plane at z = 62 mm $(120 \text{ mm} \times 120 \text{ mm})$ . The side plane is mounted to the side of the DUT at x = 55 mm (120 mm  $\times$  60 mm).

The prediction algorithm was applied to 40 combinations of additive random noise, each combination with 43 randomly selected dipole configurations to cover the hot spot, resulting in  $40 \times 43$  solutions. The dipole configurations vary from one dipole up to 238 randomly selected dipoles. The largest number of dipoles evenly spaced over the rectangular plane of  $160 \text{ mm} \times 130 \text{ mm}$  (17 dipoles in the *x*-direction and 14 dipoles in the *y*-direction with a gap of 10 mm). Fig. 3 shows the value of the quality metric  $\sigma$  calculated with (8). Three different dipole combinations which used a small number of dipoles gave lower values of the coefficient than the others which is not surprising given the simplicity of the field patterns (see Fig. 2). The combination with three dipoles in the *x* and *y* directions and a 3 mm gap, gave the minimum value of the quality metric. The variation

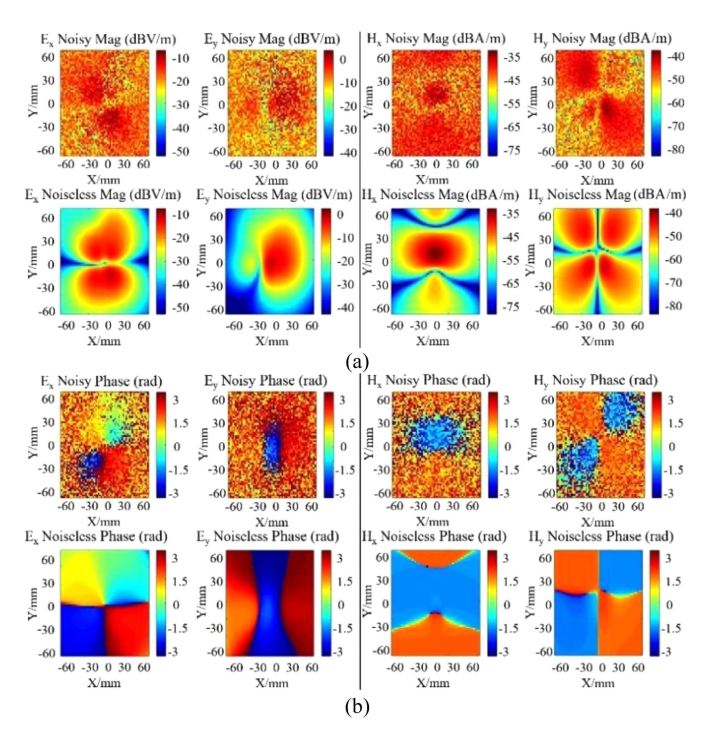


Fig. 2. Effect of adding cross-field coupling and random noise to the system on primary plane. (a) Magnitude of noisy and noiseless data for  $E_x$ ,  $E_y$ ,  $H_x$ , and  $H_y$ . (b) Phase of noisy and noiseless data for  $E_x$ ,  $E_y$ ,  $H_x$ , and  $H_y$ .

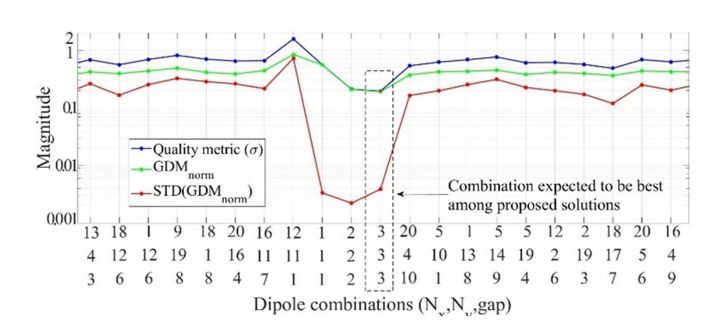


Fig. 3. Magnitude of  $\sigma$  for different dipole combinations applied to the EMI filter. The dipole combinations with the lowest value of  $\sigma$  also had the lowest values of GDM outside the measurement area.

of the GDM value (minima, maxima, and average) for the EMI filter model on the primary, secondary, and side plane for each dipole combination is shown in Fig. 4 to demonstrate that the combinations with minimum weighing coefficient also tends to provide a better representation outside of the measurement area, indicating they are a better representation of the true source. The value of GDM is highly sensitive to noise except for three middle dipole combinations (see Fig. 4). The value of GDM is also higher for other combinations than three middle combinations, especially on the side plane (see Fig. 4). The dipole combination with the lowest quality metric (calculated on the measurement plane) also has the lowest GDM at locations above and to the side of the scan plane. The fact that this combination has the lowest GDM and is robust against additive noise, i.e., it has the lowest standard deviation of GDM and helps ensure the repeatability of the result in a noisy environment.

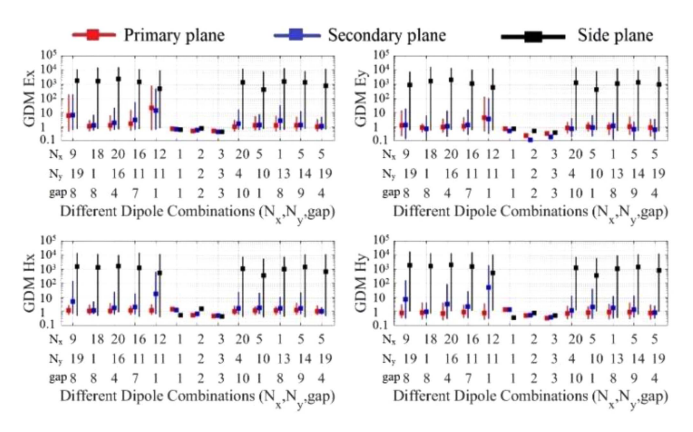


Fig. 4. Variation of the GDM value (minima, maxima, and average) for the EMI filter model on three planes.

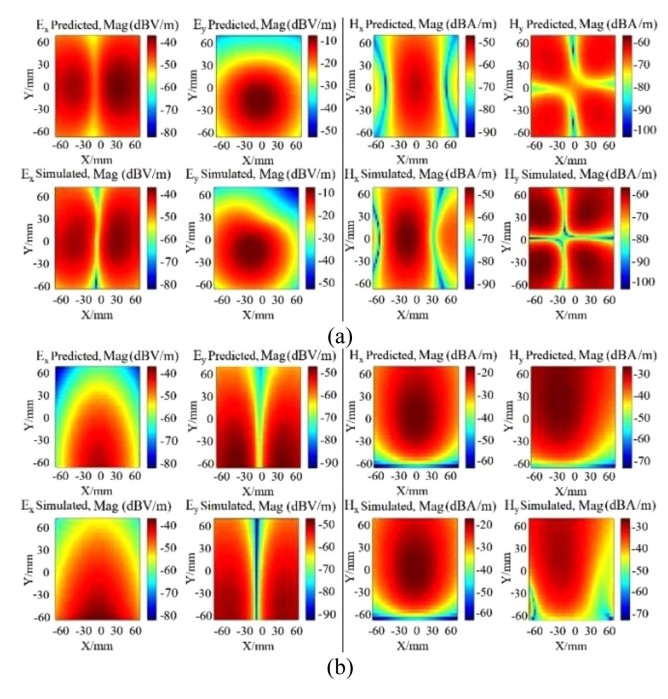


Fig. 5. Noiseless (simulated) fields and fields predicted from noisy data for the EMI filter (see Fig. 1) using the dipole combination with a minimum value of  $\sigma$  on (a) secondary plane (z = 62 mm) and (b) side plane (z = 55 mm).

Fig. 5 shows the reconstructed fields when using the combination from Fig. 3 with minimum quality metric (with three dipoles in the x and y directions and a 3 mm gap). The predicted fields are compared with simulated noiseless data at the secondary and side planes, as described earlier. The shape of the fields is reconstructed well. The value of GDM is lower than one which is considered "Fair" for FSV evaluation. A fair evaluation is not surprising given the substantial noise included in the "measured" data. The accuracy of the estimated fields depends on the number of scanning points, as well as which field components are scanned, e.g.,  $E_x$ ,  $E_y$ ,  $H_x$ , and  $H_y$ . Generally, either the electric or magnetic field (alone) can be used to reconstruct the source as long as the noise source is either electric or magnetic field dominant [1], [2], [3]. An EMI filter is a strong near magnetic

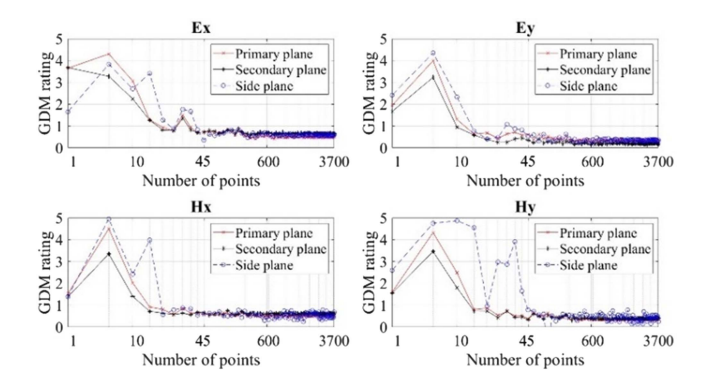


Fig. 6. FSV evaluation on different planes using only magnetic field components for prediction as a function of the number of scanning points.

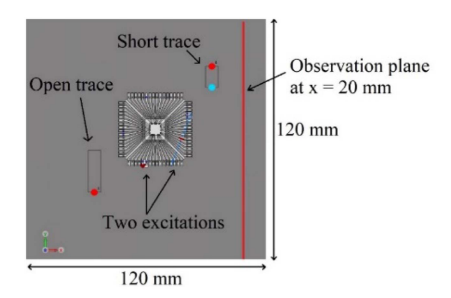


Fig. 7. IC with two nearby traces.

field source. Fig. 6 shows the values of GDM on each plane when the prediction is performed using different numbers of scanning points and only using the measured value of magnetic fields over the scan plane. As shown, for an EMI filter that has magnetic field dominated emissions, it is possible to use only around 45 measurements of only the magnetic field on a plane above the DUT (from z = 40 mm to z = 60 mm) to adequately reconstruct the source. If only the least square error was used to find a dipole combination, more combinations would be suggested as good solutions with minimum error on the primary plane, but those combinations would have very high errors on other planes like side planes (see Fig. 4).

# B. IC With Open and Short Traces

Other sources of interference may have more complex structures including both electric and magnetic field dominant sources functioning at higher frequencies. The setup shown in Fig. 7 which includes an IC and open and shorted traces was used to study these more complex scenarios. The sources shown in Fig. 7 occupy an area of 30 mm  $\times$  30 mm. The dimensions of the ground plane were 120 mm  $\times$  120 mm (0.24  $\lambda \times$  0.24  $\lambda$ at 600 MHz). Both traces were excited with a 600 MHz with a 1 V, 50  $\Omega$  port. One trace was terminated on the other side with a 1  $\Omega$  load and the other trace was left open. The IC is a commercial microcontroller in a quad-flat package. An electromagnetic model for the IC package was developed as part of the work described in [34]. The IC was mounted 0.4 mm above the perfect electric conductor (PEC) ground plane. Two pins were excited with two different 1 V,  $50 \Omega$  ports at 600 MHz. The fields generated by each stimulation source were found

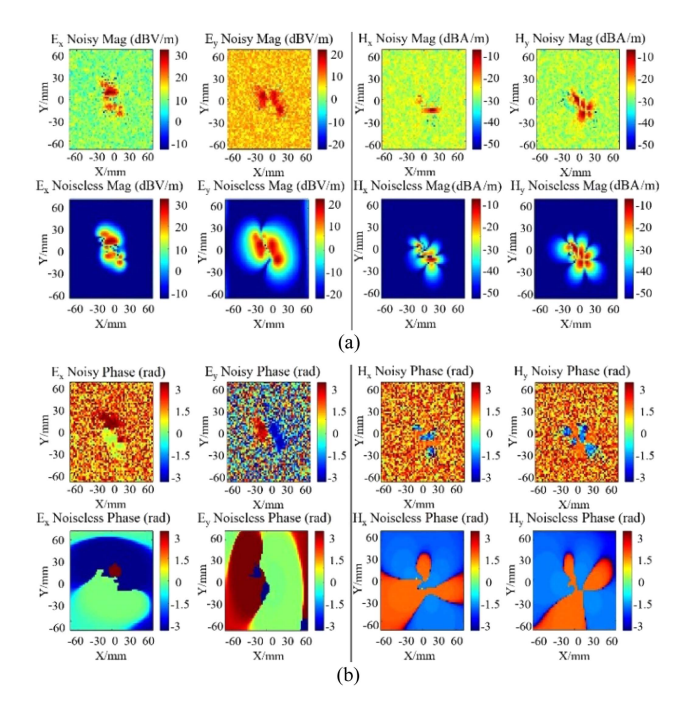


Fig. 8. Effect of adding cross-field coupling and random noise to the IC and trace setup. (a) Magnitude of noisy and noiseless data for  $E_x$ ,  $E_y$ ,  $H_x$ , and  $H_y$ . (b) Phase of noisy and noiseless data for  $E_x$ ,  $E_y$ ,  $H_x$ , and  $H_y$ .

separately and then added together to determine the overall emissions from the setup. Both magnetic and electric fields with phase were generated from these sources in CST Studio Suites [33] and used to validate methods for predicting the best dipole configuration.

Initially, the data were captured in a 120 mm  $\times$  120 mm observation plane at z=5 mm, with step size 2 mm (i.e., there were 3721 measurements of  $E_x$ ,  $E_y$ ,  $H_x$ , and  $H_y$  within the plane). Two observation planes were used to validate the results. The secondary plane is mounted in the xy plane above the scan plane at z=10 mm (120 mm  $\times$  120 mm). The side plane is mounted to the side of the DUT at x=20 mm (120 mm  $\times$  60 mm). To investigate the effects of practical limitations on reconstruction, the cross-field coupling (about 30%) and additive random noise was added to the noiseless field so that the maximum SNR  $\approx$  15 dB. Fig. 8 shows the magnitude and phase of the noiseless and noisy E- and H-fields. The noisy fields shown in Fig. 8 along with a 1.5 mm position error were used to estimate the dipole sources using (5).

Dipole source values were predicted using 40 different values of additive noise for each of the 120 different dipole configurations. The equivalent dipoles located around the hot spot occupy an 18 mm  $\times$  18 mm area (7 dipoles in the x and y directions with a gap of 3 mm) up to 84 mm  $\times$  84 mm (13 dipoles in the x and y directions with a gap of 7 mm). The quality metric  $\sigma$  was calculated with (8) and is shown in Fig. 9. As shown, the quality metric has a minimum value for the combination which uses eight dipoles in the x and y directions covering a 36 mm  $\times$  36 mm area over the source region. As shown in Fig. 10, this configuration also showed the lowest value of GDM on the primary, secondary, and side planes. Additionally, the better

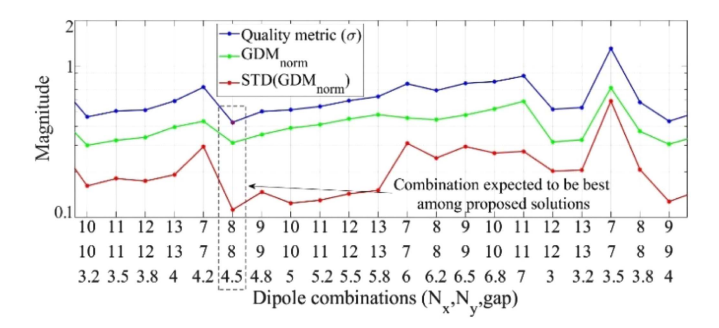
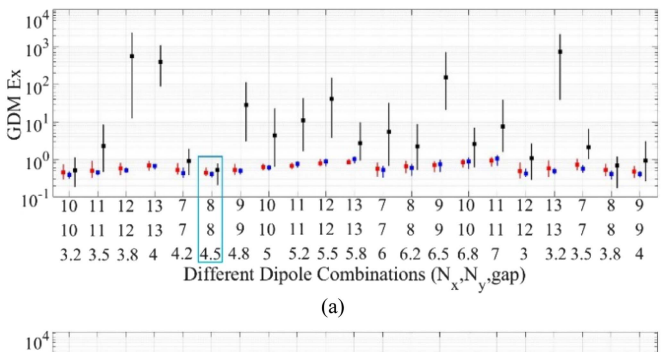
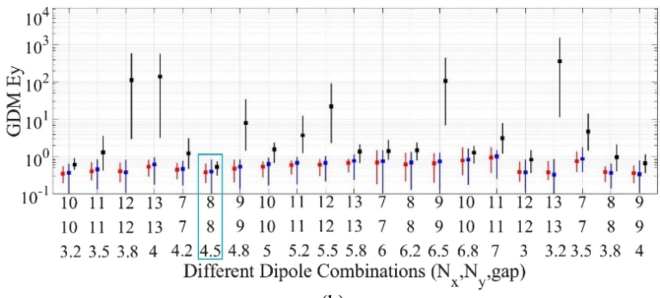
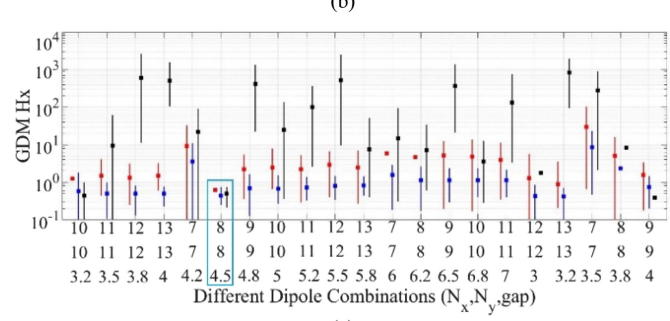


Fig. 9. Quality metric  $\sigma$  for different dipole combinations applied to the IC and traces.







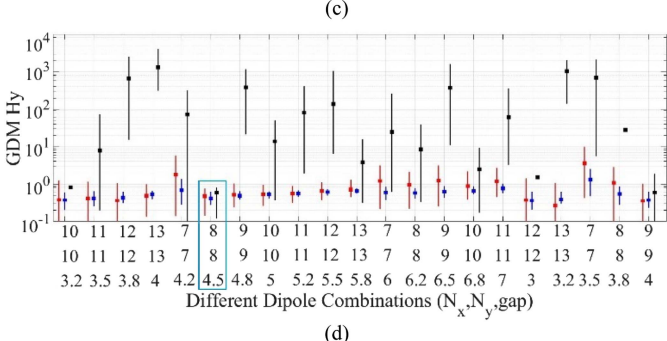


Fig. 10. Variation of the GDM value (minima, maxima, and average) for the IC and trace setup. The configuration with the minimum value of  $\sigma$  shown in the blue rectangle (red: primary plane, blue: secondary plane, black: side plane). (a) GDM  $E_x$ . (b) GDM  $E_y$ . (c) GDM  $H_x$ . (d) GDM  $H_y$ .

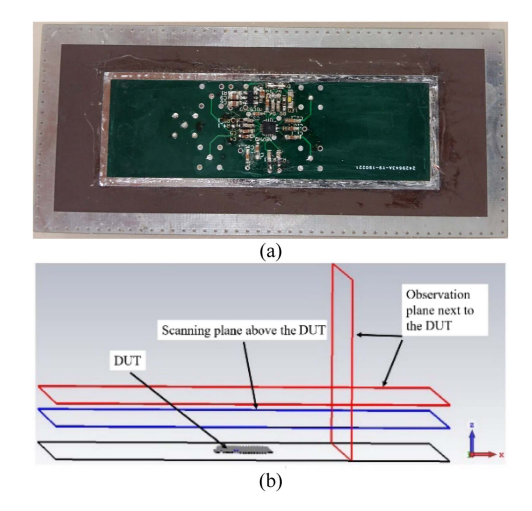


Fig. 11. Near-field scans were performed over the DUT. (a) Test board overlaid with the source surface. (b) Measurement and observation planes relative to the noise source.

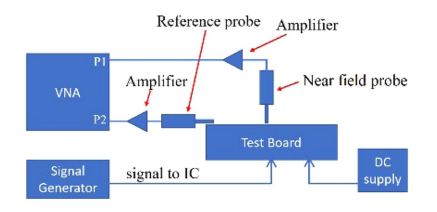


Fig. 12. Block diagram of the measurement setup.

combinations show a lower standard deviation of the GDM value over all 40 combinations of additive random noise compared to all other dipole combinations. The fact that this configuration has the lowest total GDM for the primary, secondary, and side planes is a good indication that using this dipole configuration is robust against noise and that the quality metric is useful for indicating the dipole combinations with the best repeatability in a noisy environment.

As shown in Fig. 10, a small least square error on the primary plane cannot guarantee a good field reconstruction on other planes like side plane. This is the main reason that the user cannot rely on a least square error to find a reliable dipole combination for any source reconstruction approach.

## V. VALIDATION THROUGH MEASUREMENT

Measurements of the electric and magnetic fields over a test IC board were used to validate the simulated results [33]. The IC is fed by a 5 dBm signal at 500 MHz. Near-field scans were performed at 1.5 GHz at the third harmonic of the buffer output. The x and y components of the electric and magnetic probes were measured with a near-field scan system. The probes were calibrated for accurate phase-resolved near-field scanning [34]. A vector network analyzer was used for scanning the field components and as a reference signal to obtain accurate phase-resolved results. Fig. 11 shows the DUT and the measurement planes. The measurement setup is shown in Fig. 12. The primary scanning plane was  $20 \text{ mm} \times 80 \text{ mm}$  with a step size of 1 mm (1600 measurement points) at z=2 mm. The dipoles were

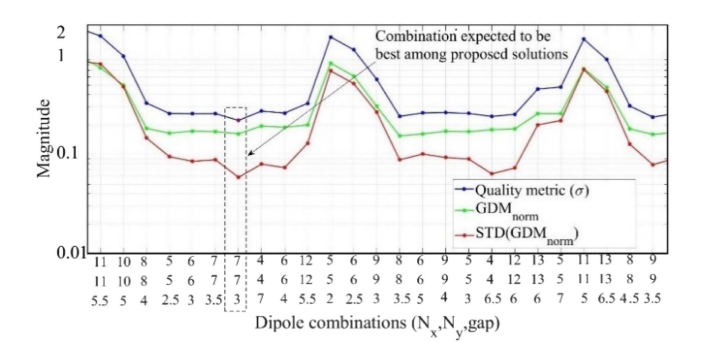


Fig. 13. Quality metric  $\sigma$  for different dipole combinations.

inferred in a plane at z = 1 mm, which is close to the physical height of the DUT. The secondary and side observation planes were at z = 6.7 mm and x = 48 mm (see Fig. 11).

Using noisy captured fields above the DUT at z = 2 mm, the prediction algorithm was repeated for 40 different combinations of additive random noise so that the maximum SNR  $\approx 15 \text{ dB}$ and with 110 different dipole configurations. The dipole configurations occupy the area from 6 mm × 6 mm (4 dipoles in the x and y directions with a gap of 2 mm) up to 84 mm  $\times$  84 mm (13 dipoles in the x and y directions with a gap of 7 mm). As shown in Fig. 13, the configuration which uses seven dipoles in the x and y directions over the 18 mm  $\times$  18 mm area had the lowest quality metric  $\sigma$ . Several dipole combinations have low GDM as they cover the source area using dipoles in x and y directions with a proper gap (see Fig. 13). The total GDM value for the DUT on the primary, secondary, and side plane is shown in Fig. 14 for the studied dipole configurations. The GDM over these additional surfaces was lowest for the configuration with minimal quality metric  $\sigma$ . Fig. 15 shows the measured and predicted fields in the yz-plane at x = 48 mm. Here, the shape of the electric fields is constructed well, and the GDM value is lower than 0.8 which is considered "Fair" in FSV evaluation [30].

If only the least square error was used to evaluate the dipole combinations, a combination with six dipoles in the x and y directions would be considered a good solution since it gives minimum error on the primary plane. However, this metric is misleading as the error in the field reconstruction on other planes e.g., the secondary or side planes are very high, and the results are not acceptable (see Fig. 14).

## VI. DISCUSSION

The proposed approach relies on the hypothesis that source configurations that are most similar to the "true" source also tend to be relatively robust to additive noise during the reconstruction process and sources that do not accurately reflect the true configuration tend to be "fragile" to small errors in the measurements. Results support this hypothesis since the proposed quality metric (designed with this hypothesis in mind) consistently found configurations that also reliably predicted fields above and to the side of the measurement plane, which were not used to estimate the source, in each of the cases tested. While further testing is needed, these results are promising.

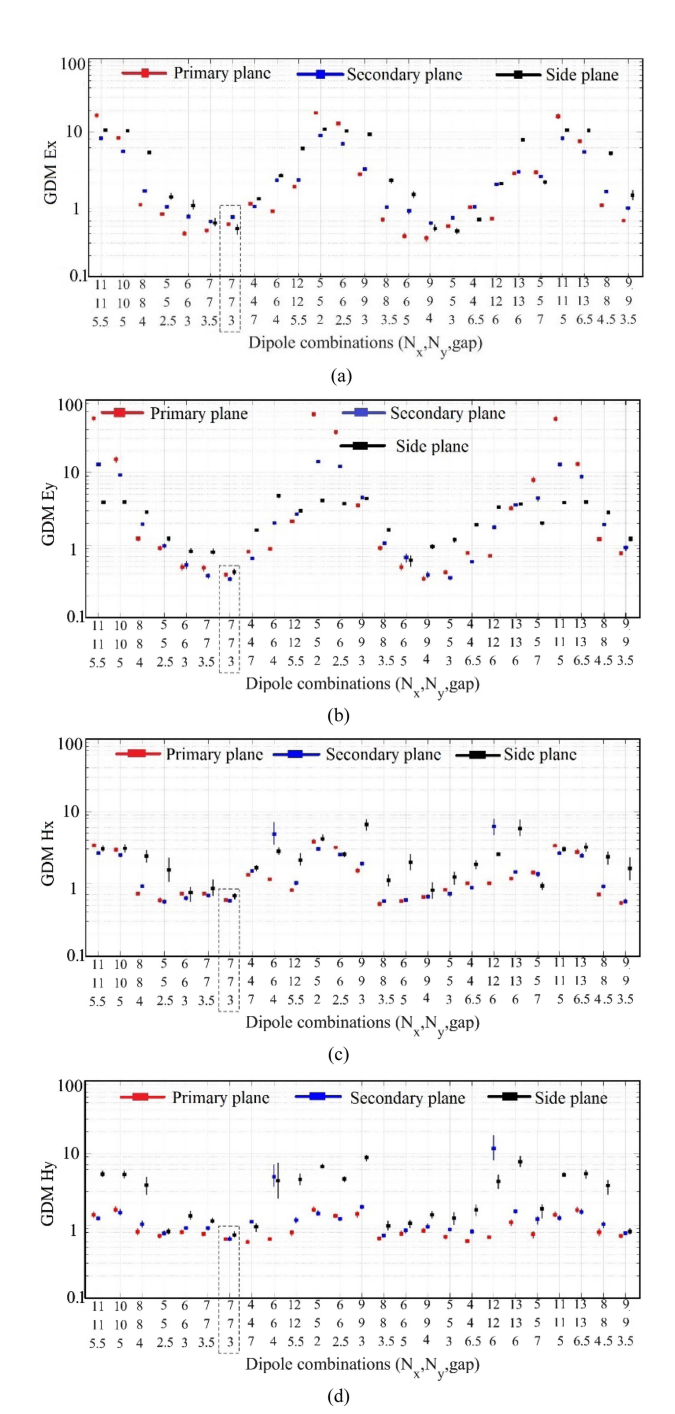


Fig. 14. Evaluation of GDM on different planes for different dipole combinations, for the setup in Fig. 14. (a)  $E_x$ . (b)  $E_y$ . (c)  $H_x$ . (d)  $H_y$ .

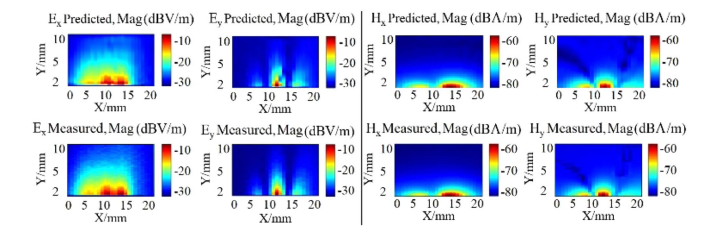


Fig. 15. Measured and predicted E- and H-fields from the DUT in Fig. 13 at x = 48 mm using the dipole combination with a minimum value of  $\sigma$ .

It should be noted that adequate testing of the robustness of the fields requires that sufficient noise be added to already noisy scan data to cause significant variations in the predicted GDM. When using real scan data, where the level of noise may not be known *a priori*, the user may need to experiment with the level of noise required to generate a good result. The noise added should be larger than the expected additive noise in the original measurement.

As shown in the plots of  $\sigma$  and of the total GDM, there are many possible dipole configurations that may give good results. The challenge for the user is determining which are good and which are poor given that all will generate a relatively low least square error on the measurement plane but may perform differently outside of the measurement plane. If only the least square error over the measurement plane were used to judge the quality of the configuration, one would tend toward solutions using a large number of dipoles that overfit the measured data. While the minimum value of  $\sigma$  provides a good indicator of which configuration gives the lowest GDM over different observation planes, other configurations with low levels of  $\sigma$  may also be good.

Near-field probes measure a weighted average of the actual field [36]. The weighting depends on the distance between the source and the probe. If the distance is small (e.g., much less than the height of the probe), then the fields within the loop (assuming a magnetic field probe) will vary strongly. If the distance is large, the fields are more-or-less uniform. One cannot correct for this effect well without explicit information about the source so that typical probe-factor assumptions will introduce additional errors in the data. While this source of error was not studied here, the fact that the quality metric  $\sigma$  does a good job of identifying source configurations that are robust to other sources of error in the measured data suggests that these configurations will also be robust to errors caused by a less-than-ideal probe compensation.

Using a CORE i5 laptop with 2.5 GHz CPU, it takes about 2 min per configuration for the method to tell the user if the proposed equivalent dipole moment for the source (see Figs. 7 and 11) is a good or bad answer. Here, more than 100 randomly selected dipole combinations were used to estimate the value of the quality metric. The time to solution could be improved using an optimization search method like GAs or machine learning, rather than testing all 100 dipole combinations, such that fewer dipole combinations would have to be tested.

In the study presented here, the quality of the reconstructed source was evaluated by considering the GDM not only in the measurement plane but also above and to the side of the measurement plane. These additional areas were considered since they are most often of concern in RFI applications [13], [18]. Other applications may also desire reconstruction of fields at other locations, for example below the measurement plane, which may be a topic for future study.

## VII. CONCLUSION

A method was proposed for finding better dipole configurations among several candidates when determining electric and magnetic fields outside the measurement area, using phaseresolved near-field scan measurements. The method is based on a quality metric, which is calculated from the GDM of near-field solutions found when estimating sources for many instantiations of additive noise on the assumption that those dipole configurations which are most robust to measurement errors will also reliably minimize the GDM in these cases. Results show the quality metric was consistently minimized for those configurations which also best represented the fields outside of the measurement plane. It is these fields that one is most often looking to estimate in RFI applications, and which are typically unavailable when estimating the equivalent source. The metric consistently identified the better source configurations even in the presence of typical measurement errors like random measurement noise in the scan data, errors in scan height, and cross-coupling between electric and magnetic field measurements. The method was applied to both simulated and measured data in a variety of scenarios where both electric and magnetic field sources dominated and was able to identify the better source configurations in each case.

#### REFERENCES

- P. Wilson, "On correlating TEM cell and OATS emission measurements," *IEEE Trans. Electromagn. Compat.*, vol. 37, no. 1, pp. 1–16, Feb. 1995, doi: 10.1109/15.350235.
- [2] Z. Yu, J. A. Mix, S. Sajuyigbe, K. P. Slattery, and J. Fan, "An improved dipole-moment model based on near-field scanning for characterizing near-field coupling and far-field radiation from an IC," *IEEE Trans. Electromagn. Compat.*, vol. 55, no. 1, pp. 97–108, Feb. 2013, doi: 10.1109/TEMC.2012.2207726.
- [3] Y. Vives-Gilabert, C. Arcambal, A. Louis, F. de Daran, P. Eudeline, and B. Mazari, "Modeling magnetic radiations of electronic circuits using near-field scanning method," *IEEE Trans. Electromagn. Compat.*, vol. 49, no. 2, pp. 391–400, May 2007, doi: 10.1109/TEMC.2006.890168.
- [4] R. Kress, Numerical Analysis. New York, NY, USA: Springer-Verlag, 1998, doi: 10.1007/978-1-4612-0599-9.
- [5] C. Wu, Z. Sun, Q. Huang, Y. Wang, J. Fan, and J. Zhou, "A method to extract physical dipoles for radiating source characterization and near field coupling estimation," in *Proc. IEEE Int. Symp. Electromagn. Compat., Signal Power Integrity*, 2019, pp. 580–583, doi: 10.1109/ISEMC.2019.8825214.
- [6] B. Wang, E. X. Liu, W. J. Zhao, and C. E. Png, "Reconstruction of equivalent emission sources for PCBs from near-field scanning using a differential evolution algorithm," *IEEE Trans. Electromagn. Compat.*, vol. 60, no. 6, pp. 1670–1677, Dec. 2018, doi: 10.1109/TEMC.2017.2769103.
- [7] T. H. Song, X. C. Wei, J. J. Ju, W. T. Liang, and R. X. K. Gao, "An effective EMI source reconstruction method based on phaseless near-field and dynamic differential evolution," *IEEE Trans. Electromagn. Compat.*, vol. 64, no. 5, pp. 1506–1513, Oct. 2022, doi: 10.1109/TEMC.2022.3181142.
- [8] W. J. Zhao et al., "An effective and efficient approach for radiated emission prediction based on amplitude-only near-field measurements," *IEEE Trans. Electromagn. Compat.*, vol. 54, no. 5, pp. 1186–1189, Oct. 2012, doi: 10.1109/TEMC.2012.2215874.
- [9] W. J. Zhao, E. X. Liu, B. Wang, S. P. Gao, and C. E. Png, "Differential evolutionary optimization of an equivalent dipole model for electromagnetic emission analysis," *IEEE Trans. Electromagn. Compat.*, vol. 60, no. 6, pp. 1635–1639, Dec. 2018, doi: 10.1109/TEMC.2018.2797265.
- [10] Y. F. Shu, X. C. Wei, R. Yang, and E. X. Liu, "An iterative approach for EMI source reconstruction based on phaseless and single-plane near-field scanning," *IEEE Trans. Electromagn. Compat.*, vol. 60, no. 4, pp. 937–944, Aug. 2018, doi: 10.1109/TEMC.2017.2756902.
- [11] L. Wang, Y. Zhang, F. Han, J. Zhou, and Q. H. Liu, "A phaseless inverse source method (PISM) based on near-field scanning for radiation diagnosis and prediction of PCBs," *IEEE Trans. Microw. Theory Techn.*, vol. 68, no. 10, pp. 4151–4160, Oct. 2020, doi: 10.1109/TMTT.2020.3006564.
- [12] W. Labiedh and J. Ben Hadj Slama, "Analysis and modeling of the magnetic near fields emited by an IGBT and by a power diode generic radiating model for active components," in *Proc. IEEE Int. Conf. Elect. Sci. Technol. Maghreb*, Nov. 2014, pp. 1–6, doi: 10.1109/CISTEM.2014.7076992.
- [13] L. Li, J. Pan, C. Hwang, and J. Fan, "Radiation noise source modeling and application in near-field coupling estimation," *IEEE Trans. Electromagn. Compat.*, vol. 58, no. 4, pp. 1314–1321, Aug. 2016, doi: 10.1109/TEMC.2016.2573160.

- [14] M. M. Hernando, A. Fernandez, M. Arias, M. Rodriguez, Y. Alvarez, and F. Las-Heras, "EMI radiated noise measurement system using the source reconstruction technique," *IEEE Trans. Ind. Electron.*, vol. 55, no. 9, pp. 3258–3265, Sep. 2008, doi: 10.1109/TIE.2008.928042.
- [15] Z. Yu, M. Chai, J. A. Mix, K. P. Slattery, and Q. H. Liu, "Inverse source solver for a high resolution near field scanner in microelectronic applications," *IEEE Trans. Compon., Packag. Manuf. Technol.*, vol. 4, no. 9, pp. 1495–1502, Sep. 2014, doi: 10.1109/TCPMT.2014.2339357.
- [16] H. Zhao, S. Tao, Z. Chen, and J. Hu, "Sparse source model for prediction of radiations by transmission lines on a ground plane using a small number of near-field samples," *IEEE Antennas Wireless Propag. Lett.*, vol. 18, no. 1, pp. 103–107, Jan. 2019, doi: 10.1109/LAWP.2018.2882132.
- [17] K. Kwak, T. Bae, K. Hong, H. Kim, and J. Kim, "Accuracy investigation of equivalent dipole arrays for near-field estimation in presence of shielding or dielectric structures," *Microw. Opt. Technol Lett.*, vol. 62, pp. 1724–1732, 2020, doi: 10.1002/mop.32223.
- [18] J. Pan et al., "Radio-frequency interference estimation using equivalent dipole-moment models and decomposition method based on reciprocity," *IEEE Trans. Electromagn. Compat.*, vol. 58, no. 1, pp. 75–84, Feb. 2016, doi: 10.1109/TEMC.2015.2496210.
- [19] H. Zhao, X. Li, Z. Chen, and J. Hu, "Skeletonization-scheme-based adaptive near field sampling for radio frequency source reconstruction," *IEEE Internet Things J.*, vol. 6, no. 6, pp. 10219–10228, Dec. 2019, doi: 10.1109/JIOT.2019.2936819.
- [20] S. Lee et al., "Analytical intra-system EMI model using dipole moments and reciprocity," in *Proc. IEEE Asia-Pac. Symp. Electromagn. Compat.*, May 2018, pp. 1169–1173, doi: 10.1109/ISEMC.2018.8393972.
- [21] X. C. Wei, Y. F. Shu, Z. K. Hu, Y. H. Zhong, and Y. W. Wang, "A summary of artificial neural networks on electromagnetic interference diagnosis," in *Proc. IEEE Int. Conf. Microw. Millimeter Wave Technol.*, May 2019, pp. 1–3, doi: 10.1109/ICMMT45702.2019.8992910.
- [22] Y. F. Shu, X. C. Wei, J. Fan, R. Yang, and Y. B. Yang, "An equivalent dipole model hybrid with artificial neural network for electromagnetic interference prediction," *IEEE Trans. Microw. Theory Techn.*, vol. 67, no. 5, pp. 1790–1797, May 2019, doi: 10.1109/TMTT.2019.2905238.
- [23] Z. K. Hu, Y. H. Zhong, Y. W. Wang, Y. F. Shu, and X. C. Wei, "Application of artificial neural network for electromagnetic source reconstruction," in *Proc. IEEE Int. Conf. Comput. Electromagn.*, Mar. 2019, pp. 1–3, doi: 10.1109/COMPEM.2019.8779236.
- [24] Z. K. Hu, Y. H. Zhong, X. C. Wei, Y. W. Wang, and Y. F. Shu, "A novel electromagnetic interference source reconstruction method based on artificial neural network," in *Proc. IEEE Int. Symp. Antennas Propag.* EM Theory, Dec. 2018, pp. 1–4, doi: 10.1109/ISAPE.2018.8634161.
- [25] J. He, Q. Huang, and J. Fan, "Dipole source reconstruction by convolutional neural networks," in *Proc. IEEE Int. Symp. Electromagn. Compat. Signal/Power Integrity*, 2020, pp. 231–235, doi: 10.1109/EM-CS138923.2020.9191529.
- [26] Q. Huang and J. Fan, "Machine learning based source reconstruction for RF desense," *IEEE Trans. Electromagn. Compat.*, vol. 60, no. 6, pp. 1640–1647, Dec. 2018, doi: 10.1109/TEMC.2018.2797132.
- [27] E. Petritoli, F. Leccese, L. Ciani, and G. Schirripa Spagnolo, "Probe position error compensation in near-field to far-field pattern measurements," in *Proc. IEEE 5th Int. Workshop Metrol. Aerosp.*, Jun. 2019, pp. 214–217, doi: 10.1109/MetroAeroSpace.2019.8869674.
- [28] S. F. Razavi and Y. Rahmat-Samii, "Resilience to probe-positioning errors in planar phaseless near-field measurements," *IEEE Trans. Antennas Propag.*, vol. 58, no. 8, pp. 2632–2640, Aug. 2010, doi: 10.1109/TAP.2010.2050421.
- [29] X. Tong, D. W. P. Thomas, A. Nothofer, C. Christopoulos, and P. Sewell, "Reduction of sensitivity to measurement errors in the derivation of equivalent models of emission in numerical computation," ACES J., vol. 26, no. 7, pp. 603–610, Jul. 2011.
- [30] A. P. Duffy, A. J. M. Martin, A. Orlandi, G. Antonini, T. M. Benson, and M. S. Wolfson, "Feature selective validation of computational electronics (CEM). Part I—The FSV method," *IEEE Trans. Electromagn. Compat.*, vol. 48, no. 3, pp. 449–459, Aug. 2006, doi: 10.1109/TEMC.2006.879358.
- [31] S. Yang, Q. Huang, G. Li, R. Zoughi, and D. J. Pommerenke, "Differential E-field coupling to shielded H-field probe in near-field measurement and a suppression approach," *IEEE Trans. Instrum. Meas.*, vol. 67, no. 12, pp. 2872–2880, Dec. 2018, doi: 10.1109/TIM.2018.2831398.
- [32] R. He et al., "Modeling strategy of EMI filters," IEEE Trans. Eelectromagn. Compat., vol. 62, no. 4, pp. 1572–1581, Aug. 2020, doi: 10.1109/TEMC.2020.3006127.
- [33] Dassault Systems, "CST microwave studio," [Online]. Available: https://www.cst.com

- [34] H. Rezaei et al., "Source reconstruction in near field scanning using inverse MoM for RFI application," *IEEE Trans. Electromagn. Compat.*, vol. 62, no. 4, pp. 1628–1636, Aug. 2020, doi: 10.1109/TEMC.2020.3006031.
- [35] J. Zhang, K. W. Kam, J. Min, V. V. Khilkevich, D. Pommerenke, and J. Fan, "An effective method of probe calibration in phase-resolved near-field scanning for EMI application," *IEEE Trans. Instrum. Meas.*, vol. 62, no. 3, pp. 648–658, Mar. 2013, doi: 10.1109/TIM.2012.2218678.
- [36] D. Paris, W. Leach, and E. Joy, "Basic theory of probe-compensated near-field measurements," *IEEE Trans. Antenna Propag.*, vol. 26, no. 3, pp. 373–379, May 1978, doi: 10.1109/TAP.1978.1141855.



Hossein Rezaei (Member, IEEE) received the B.E. degree from Islamic Azad University Najafabad Branch, Najafabad, Iran, in 2004, the M.S. degree from Shiraz University of Technology, Shiraz, Iran, in 2011, and the Ph.D. degree from Electromagnetic Compatibility Laboratory, Missouri University of Science and Technology, Rolla, MO, USA, in 2021 all in electrical engineering.

From 2020 to 2021, he was with ESDEMC Technology LLC, Rolla, MO, USA, developing electrostatic discharge (ESD) testing solutions. In April

2021, he joined Intel, and in January 2022, he joined Solidigm Technology, Folsom, CA, USA. His research interests include electrostatic discharge modeling and analysis, electromagnetic compatibility, signal integrity, RF desense, and numerical simulations.



Xin Yan (Graduate Student Member, IEEE) received the B.S. degree in applied physics from Beihang University, Beijing, China, in 2015, and the M.S. degree in electrical engineering in 2018 from Missouri University of Science and Technology, Rolla, MO, USA, where he is currently working toward the Ph.D. degree in the electrical engineering in the EMC Laboratory, Missouri University of Science and Technology, Rolla, MO, USA.

His research interests include ESD, EMI, and desense analysis.



**David J. Pommerenke** (Fellow, IEEE) received the Diploma and Ph.D. degree in electrical engineering from the Technical University Berlin, Berlin, Germany, in 1989 and 1995, respectively.

After working with Hewlett Packard for five years, he joined the Electromagnetic Compatibility Laboratory, Missouri University of Science and Technology, Rolla, MO, USA, in 2001 and changed to CTO at ESDEMC in 2019. Since 2020, he has been a Professor with the Graz University of Technology, Graz, Austria, in the EMC and RF Coexistence Laboratory.

He has coauthored more than 200 journal papers and is inventor on 13 patents. His research interests include EMC, RF interoperability, system-level ESD, electronics, numerical simulations, EMC measurement methods, and instrumentations.

Dr. Pommerenke is an Associated Editor for the IEEE Transactions on Electromagnetic Compatibility.



**Daryl G. Beetner** (Senior Member, IEEE) received the B.S. degree from Southern Illinois University, Edwardsville, IL, USA, in 1990, and the M.S. and D.Sc. degrees from Washington University, St. Louis, MO, USA, in 1994 and 1997, respectively, all in electrical engineering.

He is currently a Professor (and formerly the Chair) of Electrical and Computer Engineering with the Missouri University of Science and Technology, Rolla, MO, USA, where he conducts research with the Electromagnetic Compatibility Laboratory on elec-

tromagnetic immunity and emissions from the integrated circuit to the system level